Title	The application of LS-PIV to a small irregular river for inbank and overbank flows
Author(s)	Gunawan, Budi; Sun, Xianfang; Sterling, Mark; Shiono, Koji; Tsubaki, Ryota; Rameshwaran, Ponnambalam; Knight, Donald. W.; Chandler, Jim. H.; Tang, Xiaonan; Fujita, Ichiro
Citation	Flow Measurement and Instrumentation , 24 : 1 - 12
Issue Date	2012
DOI	10.1016/j.flowmeasinst.2012.02.001
Self DOI	
URL	https://ir.lib.hiroshima-u.ac.jp/00035029
Right	(c) 2012 Elsevier Ltd. All rights reserved.
Relation	

The application of LS-PIV to a small irregular river for inbank and overbank flows

B. Gunawan[a], X. Sun[b], M. Sterling[c], K. Shiono[d], R. Tsubaki[e], P. Rameshwaran[f], D.W. Knight[g], J.H. Chandler[h], X. Tang[i] and I. Fujita[j]

[a]Postdoctoral Research Associate, Energy-Water-System Engineering, Environmental Science Division, Oak Ridge National Laboratory, P.O. Box 2008, MS-6036, Oak Ridge, TN 37831-6036, USA

[b]Associate Professor, Key Laboratory of Northwest Water Resource, Environment and Ecology, Ministry of Education, Xi'an University of Architecture and Technology, Xi'an 710055, China

[c]Reader in Fluid Dynamics, School of Civil Engineering, University of Birmingham, B15 2TT, UK

[d]Professor of Environmental Hydrodynamics, Department of Civil and Building Engineering, Loughborough University, LE11 3TU, UK

[e]Assistant professor, Department of Civil Engineering, Hiroshima University, 739-8527, Japan

[f]Research Scientist, Centre for Ecology & Hydrology, Wallingford, OX10 8BB, UK

[g]Emeritus Professor, School of Civil Engineering, University of Birmingham, B15 2TT, UK

[h]Professor of Geomatics, Department of Civil and Building Engineering, Loughborough University, LE11 3TU, UK

[i]University Research Fellow, School of Civil Engineering, University of Birmingham, B15 2TT, UK

[j]Professor, Department of Architecture and Civil Engineering, Kobe University, Kobe 657-8501, Japan

*corresponding author: m.sterling@bham.ac.uk.

Abstract

This paper examines the feasibility of applying a mobile, large scale particle image velocimetery (LS-PIV) system to a 300m reach of a small river in order to estimate the discharge. Detailed velocity measurements at a number of locations were carried out using an acoustic Doppler current profiler (ADCP) and acoustic Doppler velocimetry (ADV) for inbank, bankfull and overbank flows. The lateral distributions of the velocity index k (i.e., the ratio of the depth-averaged velocity to the surface velocity) were found to be influenced by the secondary currents, channel vegetation and flow conditions. An attempt is made to quantify the relationship between secondary flow and the velocity index. Appropriate conclusions and advice relating to the practical use of a LS-PIV system as applied to a small river are given.

Keywords: large scale particle image velocimetery, acoustic Doppler current profiler, discharge estimation.

1. Introduction

Accurate determination of the discharge in a river is a prerequisite for a large number of applications, e.g., flood management, water quality control, reservoir operation, etc. When reliable stage-discharge relationships are not available, recourse is often made to measuring the flow using traditional methods such as current meters or dye concentrations or acoustic methods (e.g., acoustic Doppler current profiler, ADCP). Recently, there has been a growing interest in the application of remote measuring methods such as Large-Scale Particle Image Velocimetry (LS-PIV), which measure the velocity of the water surface and through some prescribed, often empirical relationship, to evaluate the discharge [1-4]. Such methods have been applied successfully to large scale rivers (i.e., channel widths 50m – 230m). See for example, [2] (Yodo River, Japan, width ~230 m), [5] (Iowa River, USA, width ~70 m) and [6] (River Arc, France, width ~50 m).

In order to estimate the discharge using LS-PIV, the time averaged streamwise surface velocity (U_s) for a given lateral distance across the channel is transformed to the corresponding depth averaged streamwise velocity (U_d) at the same lateral distance via a velocity index, k, i.e.:

$$k = \frac{U_d}{U_s} \qquad (1)$$

Knowledge of the channel geometry then enables the discharge to be estimated via integration of U_d with respect to lateral distance (y). If a power law is assumed to be representative of the velocity profile, then it is possible to show that k = 0.875 when the power exponent = 1/7. This value agrees reasonably well with data obtained from [5], who found that k = 0.85 was an acceptable approximation (i.e., the difference between the two values of k is ~ 3%).

Fig. 1 illustrates schematically the possible relationship between U_d and U_s. In Fig. 1 the idealised streamwise velocity profile is represented by a curved dashed line, with arrow vectors suggesting the

relative magnitude of the streamwise velocity. The corresponding depth averaged streamwise velocity is shown as a solid vertical black line. When the flow is predominantly 2-D (Fig. 1a), the monotonic velocity profile ensures that the surface velocity is greater than the depth averaged velocity, i.e., $k < 1$, whereas when the flow is 3-D (Fig. 1b), it is possible that the reverse occurs, i.e., $U_d > U_s$ and $k > 1$, although as will be seen later this is not always the case.

For the case of a small river, it is not unreasonable to hypothesise that due to the 3-D nature of the flow (i.e., the complex distribution of secondary currents generated by anisotropic turbulence and/or the river geometry) the velocity index will vary laterally across the channel and also between different cross sections. Hence, simply assuming a value of $k = 0.875$ would result in an incorrect estimate of the discharge. The current paper will explore the lateral variation of k in two cross sections of a 300m reach of a small river (i.e., the River Blackwater, Hampshire, UK) and will explore the relationship between k and the momentum transfer at each cross section. Detailed velocity measurements were obtained using an ADCP, an ADV and LS-PIV. The flow conditions examined corresponded to inbank, bankfull and overbank flow. In general, surface velocity measurements were undertaken five minutes after the ADCP was removed from the river to ensure that the discharge and the flow field were similar between both sets of measurements.

Section 2 of the paper outlines details relating to the experimental site, while section 3 examines data obtained by the ADCP and ADV for two cross sections. A brief introduction to the LS-PIV system is presented in section 4, in addition to the LS-PIV data collected at the two cross sections examined in section 3. An evaluation of the velocity index is undertaken in section 5. Finally, conclusions are presented in section 6.

2. Experimental site

The field data used in this paper were obtained in a 300m reach of the River Blackwater, Hampshire UK. This reach was considered an ideal location to examine the application of LS-PIV to a small vegetated river since it has been extensively studied in the past [7 – 13] and has a number of interesting features as illustrated in Fig. 2, i.e., it is a doubly meandering two stage channel with variable floodplain width. A full description of the experimental site is available in the aforementioned references but for the benefit of the reader, a brief description is provided below.

The reach upstream of that shown in Fig. 2 is dominated by urban areas which ensure that the hydrological response during periods of heavy rainfall is 'flashy'. The catchment area for the river is approximately 35km^2 and the geology mainly consists of Bracklesham Beds Sandstone, overlain by patches of Barton Sands [14]. In Fig. 2, various cross sections of interest are illustrated by a dark grey line with a corresponding number (0, 0.5, 1, 2, 5 and 6). Cross sections 0 and 0.5 are trapezoidal in nature with a concrete cross section (bed and walls). In addition, they are located close to an electromagnetic gauging station. Apart from providing a check on the discharge data obtained from the ADCP used in the current work and for providing stage data which are used to obtain the water surface slope, these cross sections are of little interest to the current project and as such will not be extensively discussed further. Furthermore, to ensure that the paper is not excessive in length, attention will be restricted to measurements collected in cross section 2 (a reasonably straight section) and cross section 5 (a hydraulically complex section where the river exhibits a meander). Finally, it is perhaps worth commenting on the 'missing' cross sections, i.e., cross sections 3 and 4. These cross sections occur on the apex of the meander between cross sections 2 and 5. Unfortunately, the stage is not routinely measured at these locations (since access to these locations during times of overbank flow was not possible) and as such cannot be used in the water surface slope calculations which are discussed below. However, other work [11, 12 and 15] have reported measurements relating to these cross sections and for the sake of consistency with previously published work the decision not to renumber cross sections 4 and 5 was taken.

Attention will be restricted to three events which occurred on 16/01/2008, 18/08/2008 and 10/02/2009. These events represent bank-full, inbank and overbank flow conditions respectively, corresponding to discharges of ~ 2.0 m^3s^{-1}, ~0.34 m^3s^{-1}, ~4.5 m^3s^{-1} respectively. In each case the water depth in the reach was monitored over a relatively long period (~10 hours) and the results are illustrated in Fig. 4, from which it can be observed that each event corresponds to a different part of the flood hydrograph. Using the data in Fig. 4, it is possible to calculate the water surface slope (S_W) which occurred during these periods of the field work. The results of this process are shown in Fig. 5 and yield S_W values of $6x10^{-4}$, $7x10^{-4}$ and 10^{-3} for the events on the 16/01/2008, 18/08/2008 and 10/02/2009 respectively. Also shown in Fig. 5 is the value of the bed slope (0.001) that was initially set when the channel was constructed. The effect of vegetation is noticeable along the reach, as illustrated by changes in water surface slope, although it is acknowledged that such changes could also be attributed to changes in the channel geometry. Fig. 6 illustrates the differences in vegetation which occurred at cross sections 2 and 5 during each of the measurements periods. The authors monitored this particular reach extensively over a 5 year period and noted some slightly changes in morphology. For example, it was observed that deposition occurred on the flood plains during the five years, 90% of which was less than 100mm; changes in the bank profile for cross sections 2 and 5 were also observed and were of the order of 20cm. However, the data presented below was collected over a 13 month period, during which no significant changes in morphology were noted.

The profiles of cross sections 2 and 5 have been measured on three previous occasions, 1995, 1997 and 2007 [15]. Fig. 3 shows the results of the survey undertaken in 2007 together with the shape of the representative cross section. The edges of each measuring cross-section were marked with wooden pegs during the three years research period so that measurements cross section could be quickly (and routinely) located. The locations of the wooden pegs were geo-referenced using a total station and twelve permanent control points that in turn were surveyed using dGPS [13]. The angle of the cross-sections 2 and 5 were found to be at 62.20 and 51.95 degrees from the (Earth) North direction. Streamwise direction in this paper is defined as the direction perpendicular to the angle of the cross-sections. However, it is also acknowledged that streamwise direction may also be defined in other

ways, such as the direction where the mean transverse velocity is equal to zero. The drawback from this is that it is likely to alter the cross-section direction for each measurement, especially in meandering cross-sections where the direction of the maximum horizontal velocity often changes with respect to its magnitude due to the centrifugal effect in such a location. Thus, the authors chose the former approach to define the streamwise direction. The ADCP data were obtained by traversing the ADCP between the two pegs that marked the measuring cross-sections using specially designed cableways system consists of two poles, a winch, a steel cable and a tethering rope [explained fully in 12]. The system ensures that the ADCP always travel in a straight direction between the two pegs. Combining this with the ADCP capability to record its position every second, the locations of the velocity data along the cross-section were geo-referenced. Knowing the locations of the ADCP data, LS-PIV data at the same locations are used for the comparison.

3. ADCP and ADV measurements

The ADCP data outlined in this paper were obtained using a modified StreamPro ADCP manufactured by Teledyne RD Instruments [16]. The ADCP was modified to include a digital compass (PNI Sensor Corporation TCM 3 Tilt-Compensated Heading Module) in order to provide reliable information relating to the orientation of the probe and to project the velocity data to the same coordinate system as that of the river geometry data. The compass has an accuracy of $\pm 0.5^{o}$ and the velocity data is considered to be accurate to within ± 0.002 ms^{-1} [16]. Full details of the modification are given in [12].

The ADCP was continuously traversed across the section, and the time taken to traverse the ADCP across one cross section was typically 90 seconds. The data presented below relate to an ensemble average of 5 and 7 traverses for cross sections 2 and 5 respectively. The sampling rate of the ADCP was set at 1Hz. The floodplain data were obtained using an ADV (Nortek 10MHz velocimeter) and sampled at a frequency of 25Hz for a period of 30s. These data were measured at a number of locations across the floodplain (depending on floodplain width), and at two points in the vertical below the free surface, i.e., 0.07m and 0.6 times the local flood plain depth). The number of measurement locations on the floodplain ranged from 8 -18. Additional work (not reported here) suggests that the results from the ADV are consistent with those of the ADCP, i.e., both sets of measurements are equally reliable [11].

Fig. 7 illustrates the contours of the streamwise velocity for each of the events obtained. With references to Figs. 7a – 7c it is noticeable that there are parts of the main channel where the ADCP is not able to measure. Notwithstanding this restriction it is felt that a reasonable understanding of the flow can be gained by examining the ADCP data. Fig. 7 illustrates that as the discharge increases, i.e., as the flow moves from inbank to over-bank, the magnitude of the maximum streamwise velocity increases from ~0.2 ms^{-1} to ~0.9 ms^{-1}. However, in all cases the region of maximum streamwise velocity occurs slightly to the right of the centre of the cross section and can extend over a significant depth, i.e., the existence of a logarithmic or power law in these regions is highly questionable. For the

overbank cases (Fig. 7c) it is evident that there is a significant lateral variation in streamwise velocity, but that at a given lateral distance, the vertical distribution of streamwise velocity appears somewhat uniform.

The streamwise velocity data obtained for the three events of concern relating to cross section 5 are shown in Fig. 8. Again it can be observed that the maximum streamwise velocity increases with the discharge. However, there is a noticeable shift in the location of this maximum towards the inner bank when the flow is overbank (c.f. Figs. 8b and 8c). This is perhaps not too surprising since at this location a proportion of the flow will be overbank and will have a tendency not to follow the curvature of the main channel (see Fig. 2). This behaviour is similar to that observed by [17] who undertook physical model studies on compound channels.

Using the ADV it was possible to measure the velocity on the floodplain, the results of which are shown in Fig. 9. Fig. 9a illustrates the 3-D nature of the flow for the event on 10/02/09 and also highlights the existence of a number of counter clockwise secondary flow cells at section 5. Fig. 9b presents the near surface velocity vectors and indicates that the lateral component of velocity varies with lateral distance. This has important implications for comparison of the data with the LS-PIV data which will be discussed later.

The main secondary flow patterns at both cross sections for all of the events examined are shown in Figs. 10 and 11. In Figs. 10 and 11, possible secondary flow circulation cells have been shown schematically. It is noticeable that there is a general qualitative agreement between all of the data shown in these figures, which suggests that the secondary circulation is reasonably well defined at cross section 5. The directions of secondary circulation in the bends of compound meandering channels with overbank flow are often observed to be in a different direction to those which arise as a result of inbank flow [18]. However, this is not observed in the current work and may be due to a weak interaction between the main channel flow and a slow upstream flow on the floodplain, the latter arising as a result of the relatively high roughness on the floodplain.

4. LS-PIV

LS-PIV is similar to conventional Particle Image Velocimetry (PIV), in that the displacement of particles within a predefined flow area is tracked and quantified. Comparing the location of particles between two successive images enables the speed (and hence the velocity) of the particles to be obtained. It is implicitly assumed that the particles are moving at the same velocity as the water and well defined marker points or "seeds", which represent the flowing water surface, are necessary for accurate velocity estimations. A variety of natural seeding materials were investigated, including sawdust and dried leaves but the preferred material eventually adopted was white biodegradable packing chips. The chips were compressed to be rectangle shape with a size of 0.01m×0.02m and a seeding density of 15-20% was obtained during the experiments. The seeds were evenly distributed on the water surface by five plastic containers mounted on a survey staff (see [19] for further details). These were inexpensive, easy to obtain, provided good image contrast and being made of starch, disintegrated within a few hours of being in contact with water. Previous work [13] has demonstrated that the current LS-PIV agrees well with data obtained from ADV measurements, i.e., differences in surface velocities between 1% and 3% were obtained (the latter technique is unable to directly measure the streamwise velocity at the surface, however, if the variation of streamwise velocity with respect to height above the channel bed is measured then it is possible to project the distribution to the water surface with reasonable confidence).

The displacement of the seeding particles was determined by computing the two-dimensional cross-correlation matrix between the interrogation area in the first image and a corresponding search patch in the second image within an image video sequence. The positional location of the highest value of the cross-correlation function was assumed to represent the displacement of the particle within the interrogation area. In order for these positions in the image plane to be transformed to a real-world object coordinates system, fixed and visible targets (0.03m x 0.05m) were placed on the floodplains at each of the cross section and their position determined using a Total Station. The instrument was located within a network of survey control points that had been established prior using differential

GPS, enabling all positions could be related to the Ordnance Survey National Grid projection. It was therefore possible to orthogonally rectify the video image and obtain surface velocity vectors in a consistent real world coordinate system across the whole site. In total, five markers were positioned on both sides of the channel and used to calculate the coordinates of image area which enabled the true coordinates of each interrogation area to be resolved. The surface velocity vector for each interrogation area was then calculated by dividing the displacement by the time interval between measured successive recordings. The final velocity vector field was obtained by time-averaging the instantaneous velocity vector fields. To remove noise within the velocity data, the probability density distribution of instantaneous streamwise velocity over the recorded time was established; data, within a 95% confidence limit were accepted while those outside the 95% confidence limit were disregarded. It was necessary in some difficult cases (i.e., where there was significant vegetation present) to employ an additional filter. This filter removed any velocities which were greater than or equal to twice the standard deviation of the measured time series.

Two mobile video cameras, each capable of being deployed within a few minutes, were used for the LS-PIV. A remote controlled digital video camcorder (Sony DCR-TRV22 High8 Handycam, DV-PAL format) was mounted on an adjustable height mast, with the tripod on the floodplain. The viewing angle of the camera was adjusted by rotating the camera horizontally and vertically using the remote control. Alternatively, a hard disk digital camcorder (JVC Everio GZ-MG275) fixed on a ladder was also used, and had the benefit of being easily moved to any location within the test reach. To obtain appropriate image coverage, it was found necessary to adjust the viewing angle in order to avoid interference with vegetation and occasionally issues associated with light reflecting from the water surface.

For the LS-PIV technique used in the current work, the spatial interrogation area was set to 0.20m x0.20m, and the spacing between two adjacent interrogation areas was approximately 0.20m. The interrogation areas were set in a straight line across the section. Typically, for each experiment there

were ~40 seeding particles in an interrogation area. At each measurement section, a 2 minute video recording was acquired at the frequency of 25 Hz.

It is perhaps worth noting that all of the experiments were undertaken during periods where the local wind velocities were low. In addition, the cross sections are well sheltered by the river banks and the surrounding vegetation. Hence, while it cannot be categorically stated that the movement of the seeding particles were not influenced by any wind, this possibility is considered remote for the experiments examined in this paper. Finally, it is noted that during all of the experiments the submersion of the seeding material was less than 15mm.

5 Lateral variation of velocity index

Section 5.1 examines the lateral variation of k across the channel in general terms and discusses the possible influence that vegetation may have on this parameter, while section 5.2 quantifies the influence of secondary flow.

5.1 Comparison of surface and depth averaged streamwised velocities

As stated in section 1, with the exception of [13], most of the research using LS-PIV, is based on data obtained in large rivers, where the assumption of the existence of a vertical distribution of streamwise velocity (e.g., a logarithmic/power law) across a large proportion of the channel is not unreasonable. Figs. 12 - 14 illustrate the lateral distribution of the streamwise depth average and surface velocities for all three events at cross sections 2 and 5. Fig. 12a highlights the effect that vegetation (illustrated in Fig. 6a) can have on the flow, i.e., the majority of the flow is directed towards the right hand side of the channel. This observation is also supported by the data of Fig. 7a. Hence, in general, the lateral distribution of depth average velocity increases with respect to lateral distance. Since the surface velocity (as obtained from the LS-PIV) remains reasonably constant, the ratio of U_d/U_s (i.e., k) also varies with respect to lateral distance. Table 1 illustrates that the average k value is 0.397 which is significantly less than the 2-D value of 0.875. This is an interesting observation since the flow is clearly 3-D at this location and for this event it would not be unreasonable to expect that the surface velocities would be smaller than the corresponding 2-D case. However, an examination of Fig. 12a reveals that the low magnitude of k can be attributed to small values of U_d which result from the presence of upstream vegetation, i.e., the submerged upstream vegetation effectively results in a two layer system, where the surface velocities are larger than those within the layer below, thus resulting in a canopy type flow.

Fig. 12b and Table 1 illustrates one of the major drawbacks with using LS-PIV during the summer, i.e., the extensive vegetation that can be found in some channels ensures that correctly seeding all of the flow is difficult. It is hypothesised that these large values of U_d/U_s arise purely from a lack of

appropriate seeding and thus demonstrate one of the difficulties of using this technique in real rivers. The large variations in k suggest that in channels which have a large amount of vegetation, the current version of the LS-PIV is not sufficiently accurate to be used for discharge estimation. The values of k reported in Table 1 are obtained from the set $0 < k < 2$, since values outside this set are attributed to a lack of seeding, (i.e., where particles were not transported into the wake and dead zones due to flow separation when seeding particles were released in the river upstream of vegetation).

Fig. 13 illustrates the lateral variation of U_d, U_s and k (i.e. U_d/U_s) for inbank conditions during the winter and again support the results illustrated in Figs. 7b and 8b. In Fig. 13b, the large variations of k near the channel banks can be attributed to a lack of seeding in this area. However, these areas represent a small proportion of the flow and as such the error in the discharge estimation (or the average value of k) will be small. Figs. 10 and 11 illustrate that at both cross sections the flow is 3-D. However, there are different mechanisms driving this secondary flow; at the bend (cross section 5) there is a strong component of secondary flow which arises due to flow moving around a bend (i.e., secondary flow of the first kind, see [19]) whereas in the straight section (section 2) such features are not present and the secondary flow arises largely from the anisotropy of turbulence. However, the magnitude of the secondary flow at cross section 2 suggests that there is an element of the first kind of secondary flow which probably arises as a result of the shape of the river upstream of this cross section (see Fig. 2).

Finally, Fig. 14 illustrates the data for the overbank case. Similar to the results of Fig. 13, the results pertaining to cross section 5 illustrate a more uniform distribution of k across a large region of the channel (i.e., where the majority of the flow occurs). It is suggested that this behaviour may be due to the momentum transfer arising as a result of the secondary flow (c.f Figs. 10c and 11c). However, unlike the previous case, there is also additional shear due to the interaction of the floodplain flow with the main channel [17, 20]. It is postulated that this additional mixing is perhaps the reason why the average k value in Table 1 differs between bankfull and overbank full conditions at cross section 5.

5.2 Variation of *k* with respect to secondary flow and hydraulic mean depth

Quantifying the effect of secondary flows is not straightforward and as mentioned above can be highly subjective (open to interpretation). Furthermore, the exact definition of what constitutes secondary flow is not straightforward since in a natural river there are a number of factors which could result in the transfer of momentum at a particular cross section. In terms of interpreting the physical behaviour numerically, the exact definition can also depend on the numerical model one wishes to employ. In an attempt to try and simplify the analysis while at the same time ensuring a robust and reliable framework is used, recourse will be made to the definition adopted by Shiono and Knight [21]. The Shiono and Knight approach is considered appropriate for the current analysis since their work enables the lateral distribution of depth averaged streamwise velocity across a channel at a particular cross section to be predicted, i.e., it is consistent with the data examined above. The essence of the Shiono and Knight model is that any prismatic cross section may be discretized by a series of linear elements, thus producing panels with either a flat or a sloping bed. Within each panel, an estimate of the local friction, turbulent mixing and secondary flow is required. It is the latter which is of interest to the current analysis and is defined as:

$$\Gamma = \frac{\partial}{\partial y}[H\rho(UV)_d] \tag{2}$$

where y is the lateral distance across the channel, H is the local depth of flow, ρ is the density, U is the local streamwise velocity (at a given height above the channel bed), V is the local lateral velocity (at a given height above the channel bed) and $(UV)_d$ represents an average of the product UV with respect to the local water depth. Fig. 15 is a schematic illustration of the relationship between U, V, and $(UV)_d$, while Fig. 16 shows how these parameters conceptually relate to Γ and the secondary flow cells.

Figs. 17 - 19 illustrate the average variation of $(UV)_d$ across the channel which was obtained by calculating the local value of $(UV)_d$ and using a moving average filter based on the previous eleven data points. For ease of comparison, the variation of k with respect to lateral distance is also shown in

Figs. 17 – 19 (the dotted linear lines in Figs. 17 – 18 and the corresponding values of Γ (i.e., "a. -10", "b. 46" etc.) will be discussed subsequently). Fig. 16a illustrates that the magnitude of $(UV)_d$ is close to zero across a large part of the channel (1m < y < 5m). However, it is noticeable that the largest fluctuations in $(UV)_d$ occur as k tends towards unity. It is also noticeable in Fig. 17b, that the relatively large fluctuations of $(UV)_d$ (i.e., 2m < y < 4m) occur when k is greater than or equal to unity. (In section 5.1, these large values of k were postulated to occur as a result of insufficient seeding. While the authors feel that this is still the case, the corresponding variation in $(UV)_d$ in interesting to note). Similar results can also be observed in Figs. 18 and 19, i.e., when k is either greater than unity, there are significant fluctuations in $(UV)_d$. This is perhaps not too surprising since Figs. 10 and 11 illustrate that the secondary flows during these events are reasonably well defined. Indeed, it is evident from Fig. 10a that the flow structures are weakly defined which explains the lack of variation in $(UV)_d$ illustrated in Fig. 17a.

Fig. 20 illustrates the relationship between $\overline{|\Gamma|}$ (i.e., the average value of Γ irrespective of sign) and hydraulic mean depth (H_m). The value of $\overline{|\Gamma|}$ is based on the previously calculated $(UV)_d$ values at each depth-averaged point (local value) along the lateral direction and is calculated using equation (2). The hydraulic mean depth corresponds to the ratio between cross sectional area and water surface width, for each cross section for each event. Fig. 20 shows that $\overline{|\Gamma|}$ increases almost linearly with H_m, indicating that the secondary flow's strength increases with water level. As shown in Fig. 20, a regression analysis yields a similar value of the gradient for both cross sections' data, i.e., 0.005 and 0.0042 for sections 2 and 5 respectively. It is interesting to note that both cross-sections also have an approximately similar magnitude of $\overline{|\Gamma|}$ for each event, ~20, ~60 and ~120 for the inbank, bankfull and overbank flow conditions respectively. Fig 21 illustrates the relationship between $\overline{|\Gamma|}$ and $|\Gamma|_{max}$ for each cross section for each event. The arrows in Fig. 21 indicate the direction of increasing water depth between each event. Fig. 21 shows that there is an approximately linear relationship between $|\Gamma|_{max}$ and $\overline{|\Gamma|}$, and hence, H_m. However, it is acknowledged such a relationship is likely to be site specific.

Fig. 22 illustrates the relationship between the velocity index and $\overline{|\Gamma|}$ normalised by H_m. It is clear from Fig. 22 that the distinct relationship between k and $\overline{|\Gamma|}/|\Gamma|_{\max}$ is complex. However, it is perhaps not unreasonable to suggest that the relationship is dependent on the flow mechanism responsible for generating the bulk of the momentum transfer. For example, when the flow is either inbank or bankfull at cross section 2 (i.e., when the streamwise mean vorticity is generated (to a large extent) as a result of the anisotropy between the Reynolds stresses arising from the square of lateral and vertical velocity components), the velocity index is below unity. However, when the main exchange of momentum is not due to the aforementioned difference in Reynolds stresses, i.e., these exchanges (predominantly) occur due to the formation of a shear layer with spanwise vorticity (see section 5 data in Fig. 22), the trend in the relationship between k and $\overline{|\Gamma|}/|\Gamma|_{\max}$ is significantly different.

As stated previously, it is common to discretize a cross section into a number of linear elements and use local values of Γ in each element rather than a global, average (or maximum) value. In Figs. 18a, 21a and 22b, it is possible to identify regions where the variation of $(UV)_d$ is approximately linear. Such regions are conceptually associated with the secondary flow cells illustrated in Fig. 16 and enable local values of Γ to be calculated. The magnitude of these values are illustrated in each figures for each of the different regions identified (i.e., a-h in Fig. 18a a-d in Figs. 19a and 19b) and indicates that there is a significant variability within each cross section. In addition, this analysis suggests that initial pattern (and number) of cells is more complex that that illustrated in Figs. 10 and 11. However, as stated previously inferring secondary flow cells from velocity vector diagrams is fraught with difficulty, hence, the previous trends in Figs. 10 and 11 have not been altered.

6. Conclusions

One of the main drivers for the current work was to explore the lateral variation in the velocity index which would ultimately provide an insight into the feasibility of using LS-PIV in a small river in order to estimate the discharge. Previous work [5] has illustrated that the k ratio for large rivers is reasonably consistent and attains a value of ~0.875. However, the results of the current work have shown that this is not necessarily the case for a small meandering river. The following conclusions can be drawn with respect to the reach examined:

- the ratio of the depth average streamwise velocity to the surface streamwise velocity (i.e., k) can vary significantly between different cross sections,
- the value of k can vary significantly within the same cross section depending on the type of flood event and season, (c.f. cross section 2 inbank and overbank flow),
- the above two bullet points suggest that k is highly dependent on the structure of the flow field which is influenced by the cross sectional shape of the reach, local vegetation and stage.
- for all of the events examined the flow has been shown to be 3-D which explains why the 2-D value of 0.875 is not appropriate,
- the relationship between k and the secondary flow is complex which illustrates that for a small river it is not feasible to obtain detailed information of the flow structures in the river by simply monitoring the surface velocities,
- for practical purposes, a value of $k = 1.0$ could be adopted in order to estimate the discharge in a small river provided that the cross section is chosen appropriately, i.e., a location where there is strong secondary circulation (e.g., at an apex of a bend) or at a location where the turbulence within the reach is maximised.

7. Acknowledgements

The authors are grateful to the UK Engineering and Physical Sciences Research Council who funded this research under the auspices of grant EP/E002250/01. The writers also wish to acknowledge the support given by Environment Agency for England and Wales and the Blackwater Valley Countryside Partnership.

Table 1. Variation of average *k* values with respect to cross section and flow event.

Event	Cross section 2	Cross section 5
Inbank (18/8/2008)	0.397	1.175
Bankfull (16/01/2008)	0.862	1.028
Overbank (10/2/2009)	0.989	1.066

References

[1] Fujita I. and Komura S. (1994). Application of video image analysis for measurements of river-surface flows. *Proceedings in Hydraulic Engineering, JSCE,* 1994, 38, 733-738 (in Japanese).

[2] Fujita I., Muste M. and Kruger A. (1998). Large-scale Particle Image Velocimetry for flow analysis in hydraulic engineering applications. *Journal of Hydraulic Research*, 1998, 36(3), 397-414.

[3] Fujita I. and Aya S. (2000). Refinement of LSPIV technique for monitoring river surface flows. *Joint Conference on Water Resource Engineering and Water Resources Planning and Management*, Minneapolis, Minnesota, USA.

[4] Fujita I. and Tsubaki R. (2002). A novel free-surface velocity measurement method using spatio-temporal images. *Proceedings Hydraulic Measurements & Experimental Methods, ASCE-IAHR Conference*, Estes Park, CO, USA.

[5] Creutin J. D., Muste M., Bradley A. A., Kim S. C. and Kruger A. (2003). River gauging using PIV technique: proof of concept experiment on the Iowa River. *Journal of Hydrology*, 2003, 277, 182 – 194.

[6] Jodeaua M., Hauetb A., Paquiera A., Coza J. Le and Dramaisa G. (2008). Application and evaluation of LS-PIV technique for the monitoring of river surface velocities in high flow conditions. *Flow Measurement and Instrumentation*, 19(2), 117-127.

[7] Lambert, M. F. and Sellin, R. H. J. (1996). Velocity distribution in a large-scale model of a doubly meandering compound river channel. *Proceedings of the Institution of Civil Engineers, Water Maritime and Energy,* 118, 10-20.

[8] Naish, C. and Sellin, R. H. J. (1996). Flow structure in a large-scale model of a doubly meandering compound river channel. In *Coherent Flow Structures in Open Channels*, 631-654 (Eds P. J. Ashworth, S. J. Bennett, J. L. Best and S. J. McLelland). J. Wiley.

[9] Sellin, R. H. J., Wilson, C. A. M. E. and Naish, C. (2001). Model and prototype results for a sinuous two-stage river-channel design. *Journal of the Chartered Institution of Water and Environmental Management,* 15(3): 207-216.

[10] Sellin, R. H. J. and van Beesten, D. P. (2004). Conveyance of a managed vegetated two-stage river channel. *ICE Journal of Water Management,* 157(1): 21-33.

[11] Gunawan, B., Sun, X., Sterling, M., Knight, D. W., Shiono, K., Chandler, J., Rameshwaran, P., Wright, N. G., Sellin, R. H. J., Tang, X. & Fujita, I. (2008). An integrated and novel approach to estimating the conveyance capacity of the River Blackwater. In *International Conference on Hydroscience and Engineering,* Nagoya, Japan.

[12] Gunawan, B., Sterling, M. and Knight, D. W. (2010). Using an acoustic doppler current profiler in a small river. *Water and Environment Journal.* Vol. 24 no. 2 pp 147-158. doi: 10.1111/j.1747-6593.2009.00170.x.

[13] Sun, X., Shiono, K., Chandler, J. H., Rameshwaran, P., Sellin, R. H. J and Fujita, I. (2010). Discharge estimation in a small irregular river using LSPIV. Proceedings of the ICE, Water Management, 163(5), 247 –254.

[14] Clarke, A., Hughes, T., Hensler, A. and Jenkin, P. (2007). River Blackwater Flood Study: Final Flood mapping Report. Peter Brett Associates, Reading.

[15] Gunawan, B. (2010). A study of flow structures in a two-stage channel using field data, physical modelling and numerical modelling. PhD thesis, the University of Birmingham, Birmingham, UK.

[16] StreamPro ADCP datasheet [online]. www.rdinstruments.com. Last accessed 10th January 2011.

[17] Shiono, K and Muto, Y (1998) Complex flow mechanisms in compound meandering channels with overbank flow. Journal of fluid mechanics, 376, 221-261.

[18] Chandler, J.H., Wackrowa, R., Sun, X., Shiono, K. and Rameshwaran, P.(2008). Measuring a dynamic and flooding river surface by close range digital photogrammetry. In the International Archives of the Photogrammetry, Remote Sensing and Spatial Information

Sciences, xxxvii(B8), CHEN Jun, JIANG Jie, Ammatzia PELED, Beijing, 3rd July 2008, 211-216, ISSN: 1682-1750, [Also on CD-ROM].

[19] Perkins, H. J. (1970). The formation of streamwise vorticity in turbulent flow. Journal of Fluid Mechanics, 44, 721-740.

[20] Shiono, K., Muto, Y., Knight, D. W., and Hyde, A. F. L (1999). Energy losses due to secondary flow and turbulence in meandering channels with overbank flows. Journal of Hydraulic Research, 37(5), 641-664.

[21] Shiono, K. and Knight, D.W. (1991). Turbulent open-channel flows with variable depth across the channel. Journal of Fluid Mechanics, Cambridge University Press, 222 617-646.

[22] Knight, D.W., Omran, M. and Tang, X. (2007) Modelling depth-averaged velocity and boundary shear in trapezoidal channels with secondary flows, Journal of Hydraulic Engineering, ASCE, Vol. 133, No. 1, January, pp. 39-47.

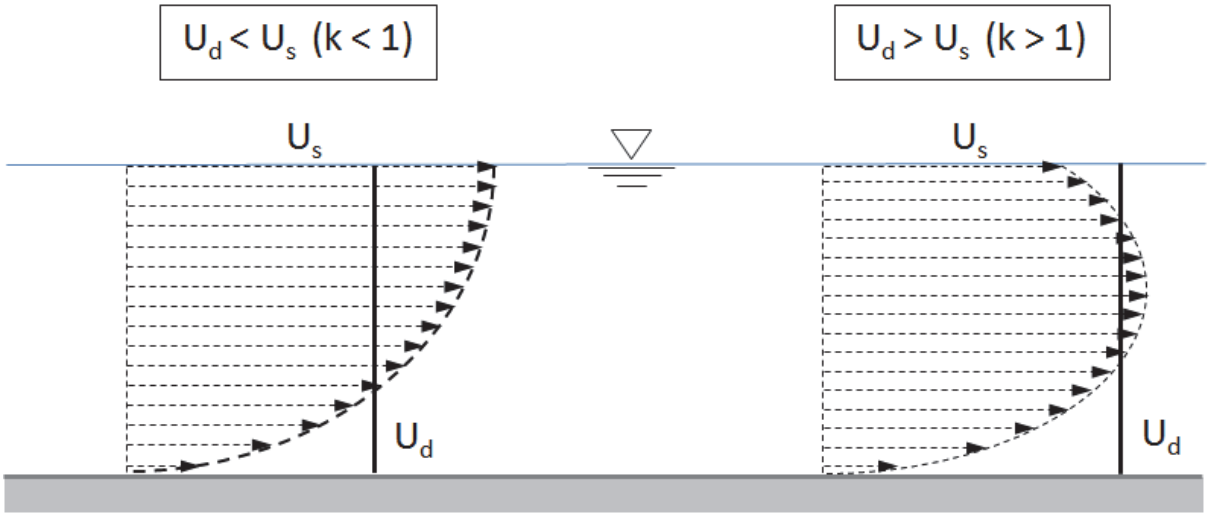

Fig. 1. A schematic illustrating the possible relationship between the depth averaged and surface streamwise velocities.

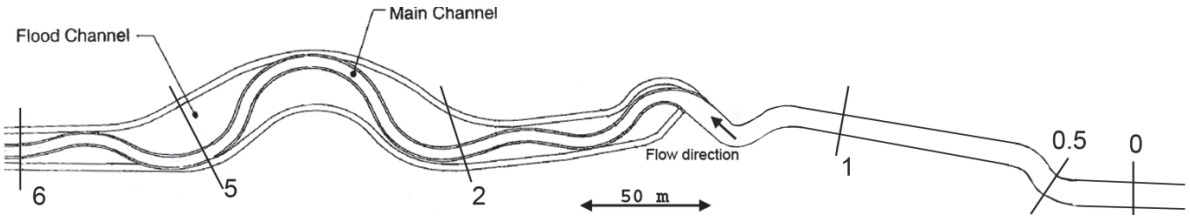

Fig. 2 Cross section and staff gauge locations.

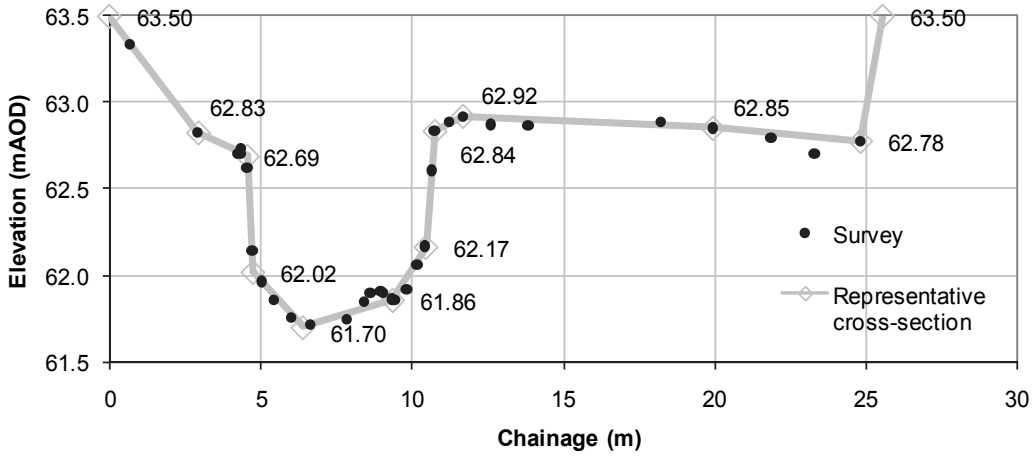

(a) cross section 2

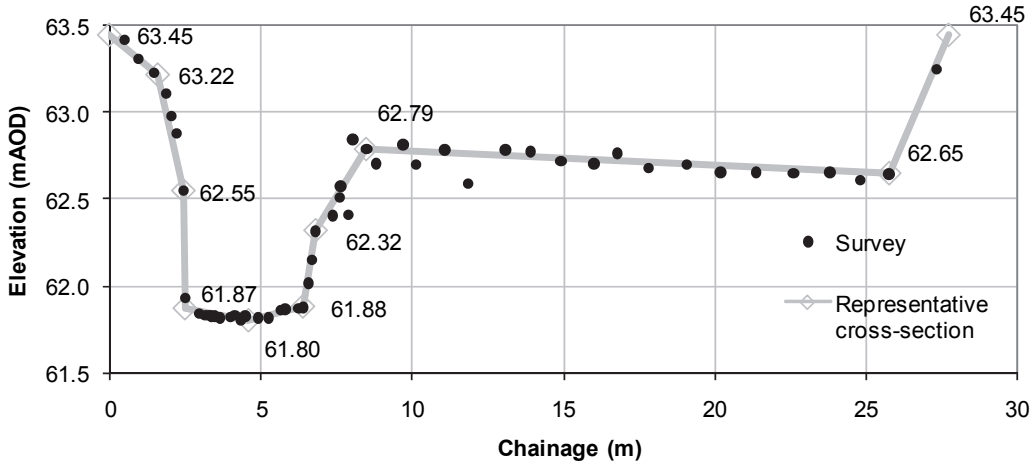

(b) cross section 5

Fig. 3 Cross sectional profiles.

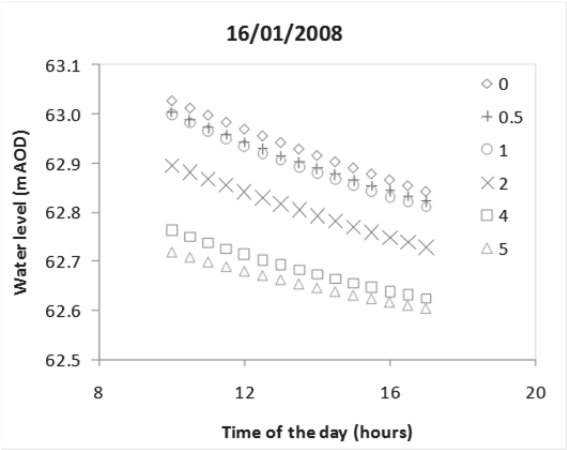

(a) 16/01/2008 data

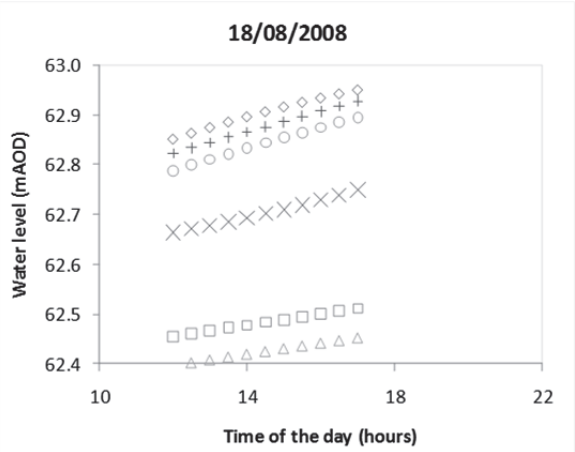

(b) 18/08/2008 data

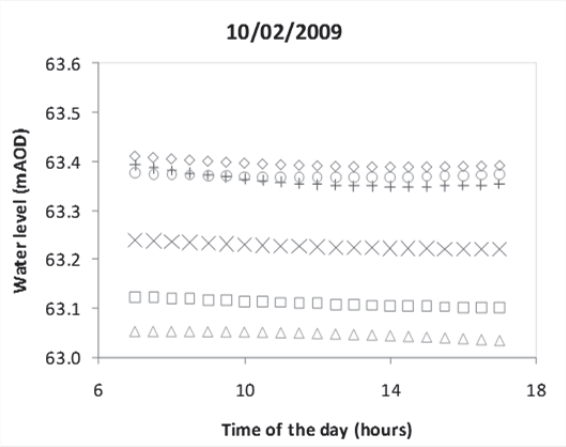

(c) 10/02/2009

Fig. 4 Water level elevations relating to the three fieldwork campaigns.

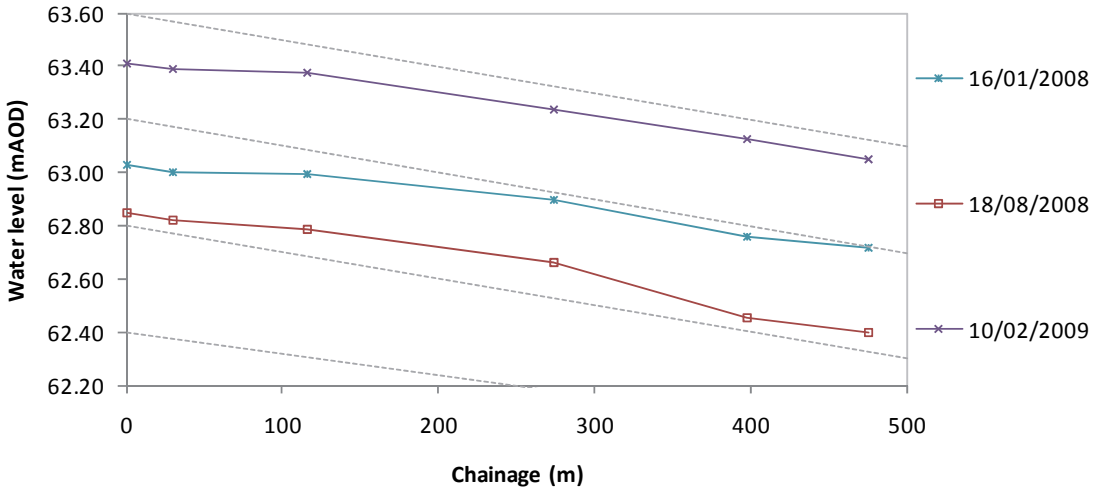

Fig. 5 Water level elevations at six measurement stations during five fieldwork campaigns.

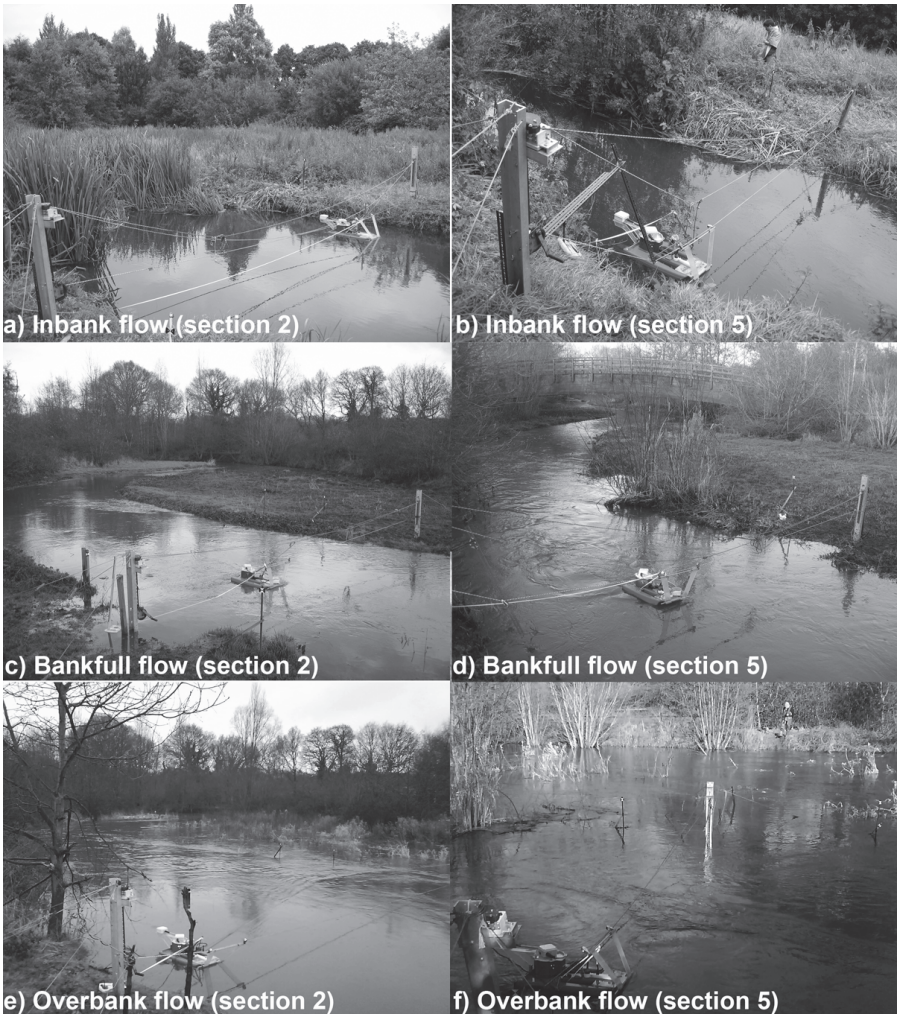

Fig. 6. Photographs illustrating changes in vegetation with respect to time (flow event).

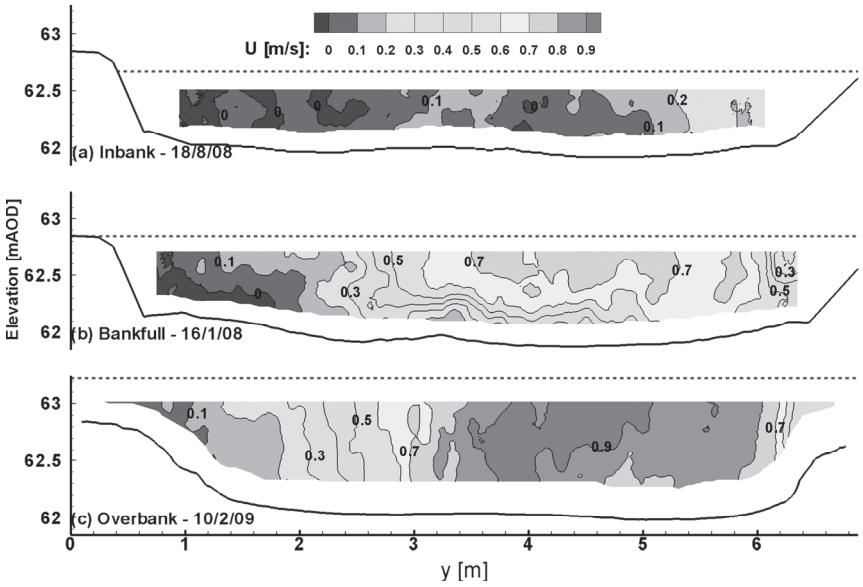

Fig. 7. Contours of the streamwise velocity component (*U)* for the three dates of concern – cross section 2. (y is the lateral distance from the left hand bank looking downstream).

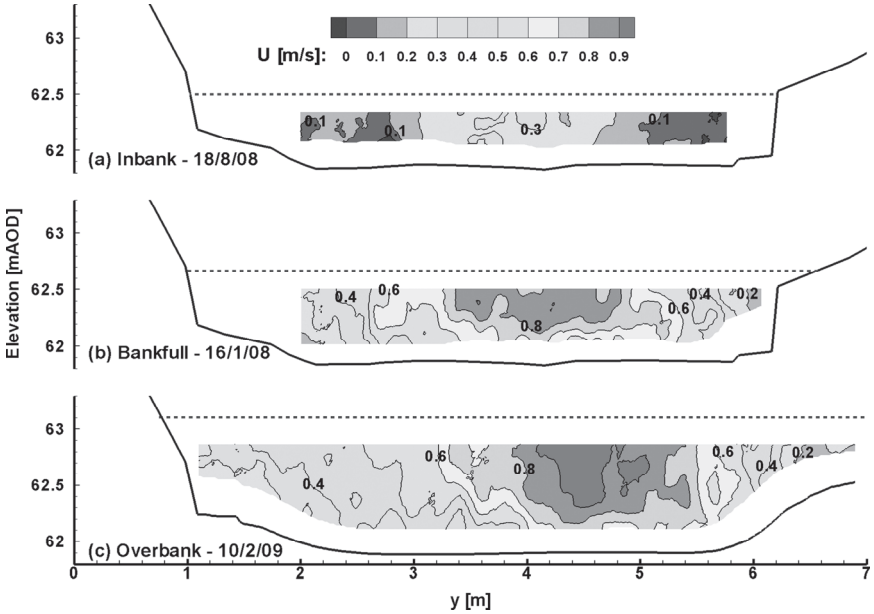

Fig. 8. Contours of the streamwise velocity component (*U)* for the three dates of concern – cross section 5. (y is the lateral distance from the left hand bank looking downstream).

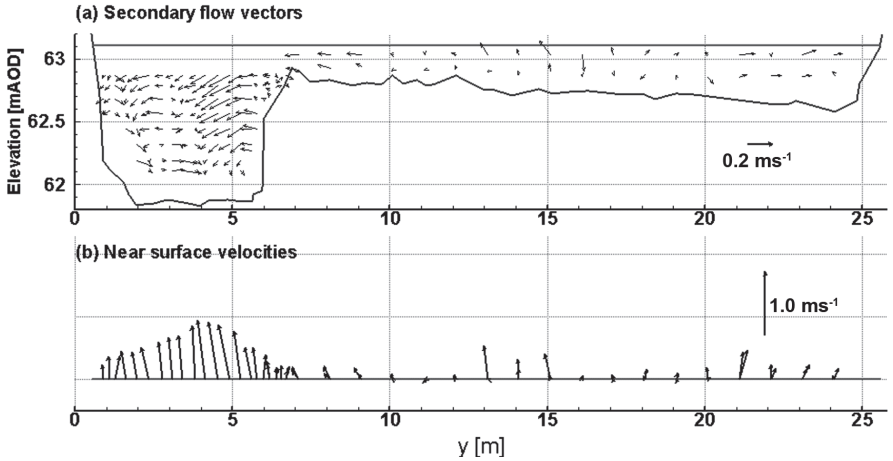

Fig. 9. Velocity vectors at cross section 5 for 10/02/09 flood event.

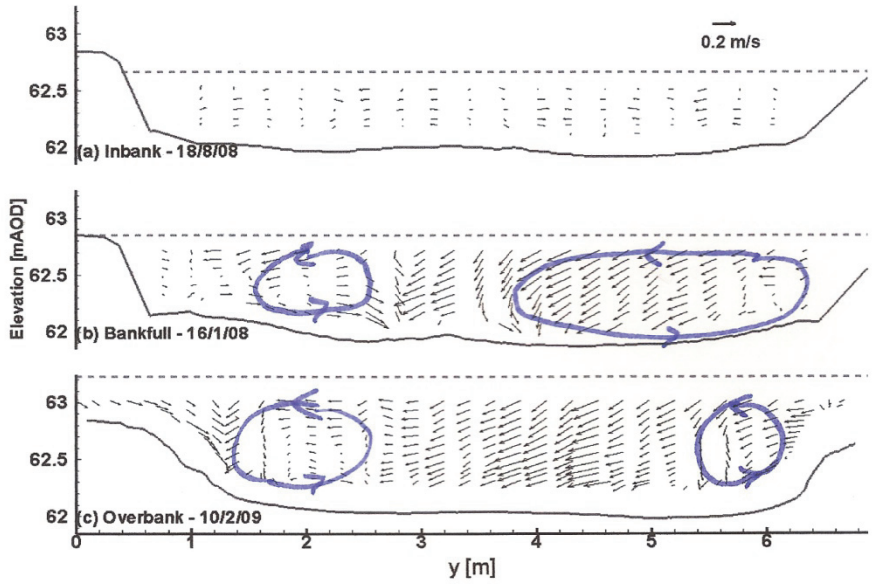

Fig. 10. Secondary flow circulations for the three flow events – cross section 2.

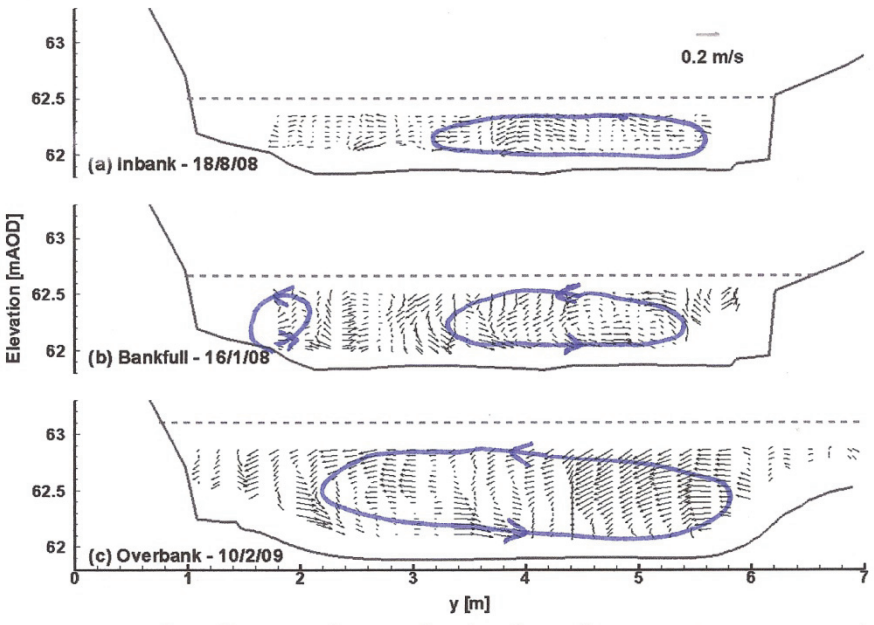

Fig. 11. Secondary flow circulations for the three flow events – cross section 5.

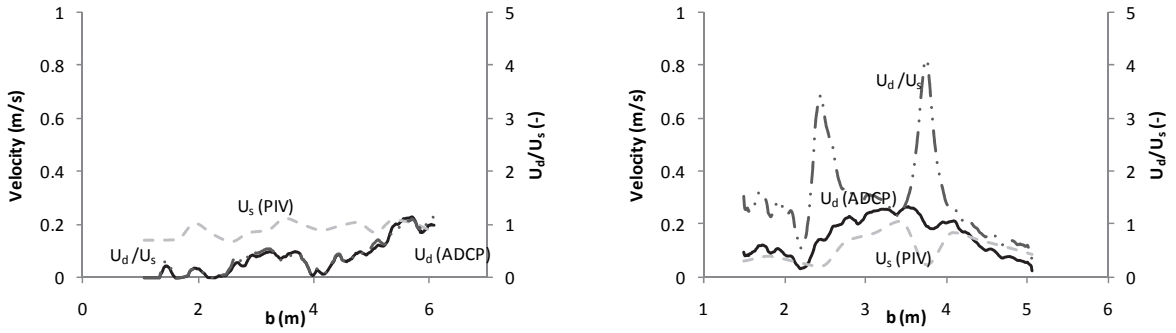

(a) section 2 (b) section 5

Fig. 12 Comparison of ADCP streamwise velocity and PIV surface velocity for 18/8/2008. (U_d (ADCP) – solid line, U_s (PIV) dashed grey line, U_d/U_s –doubled dashed grey line).

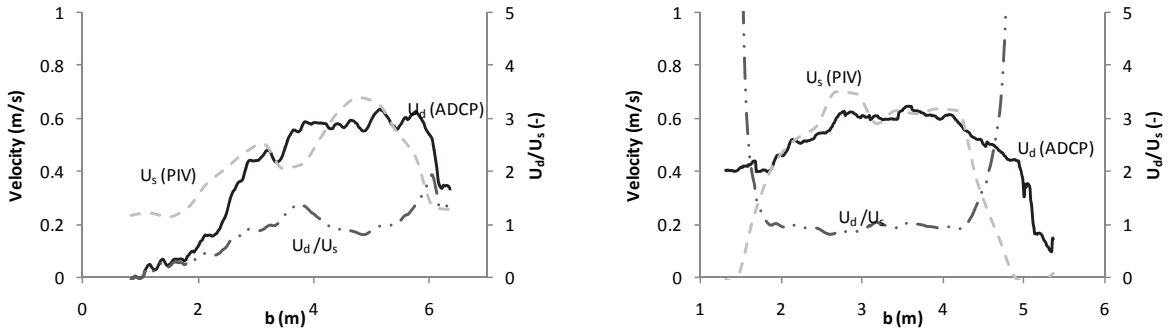

(a) section 2 (b) section 5

Fig. 13 Comparison of ADCP streamwise velocity and PIV surface velocity for 16/1/2008.

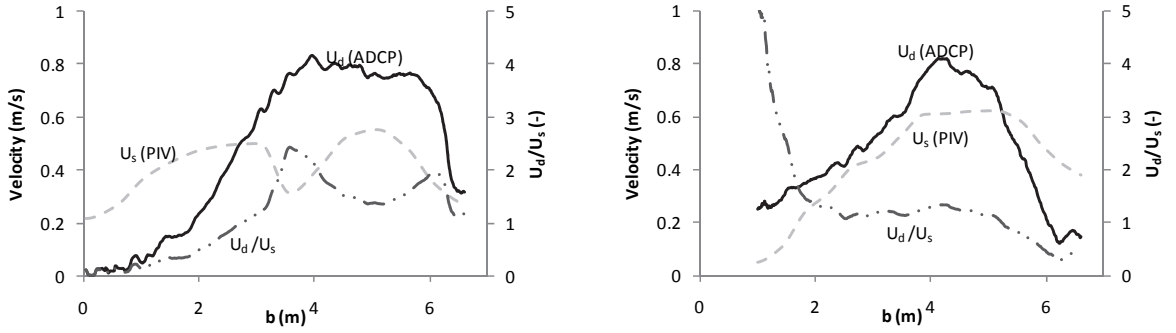

(a) section 2 (b) section 5

Fig. 14 Comparison of ADCP streamwise velocity and PIV surface velocity for 10/2/2009.

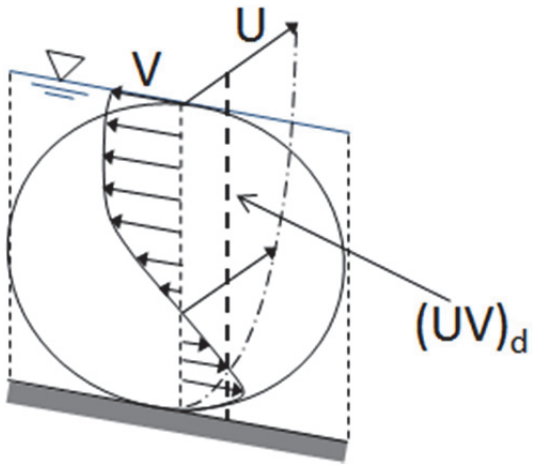

Fig. 15. Depth-averaged secondary flow [22]

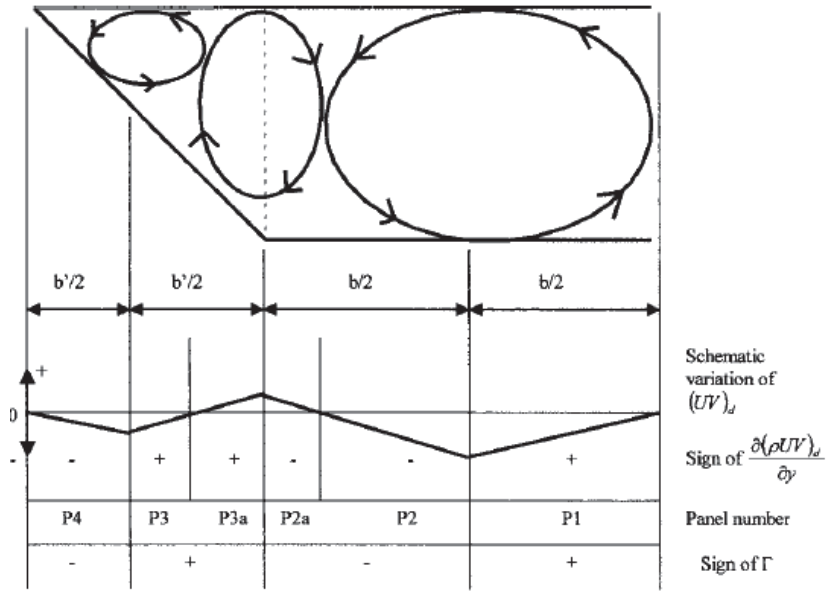

Fig. 16. Depth-averaged secondary flow parameter [22].

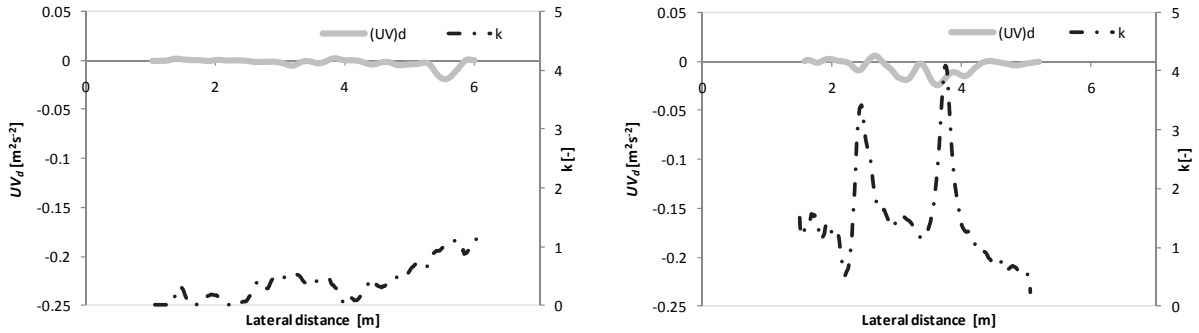

(a) section 2 (b) section 5

Fig. 17. Lateral variation of $(UV)_d$ and k for 18/08/2008.

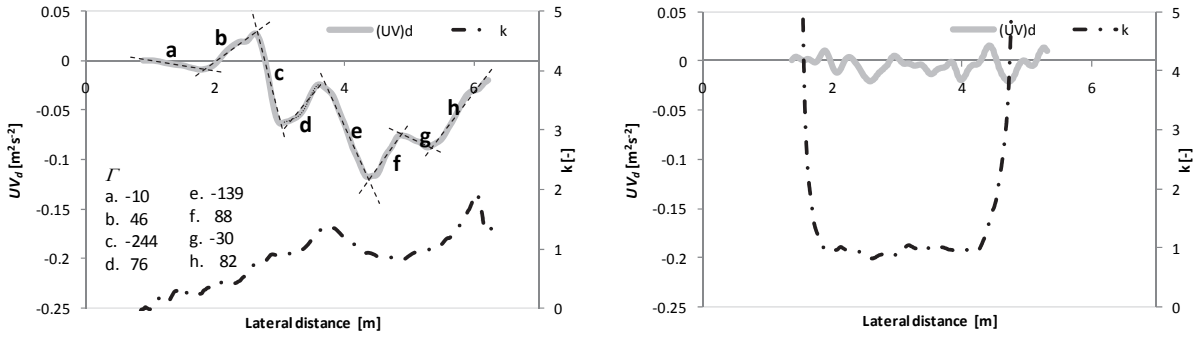

(a) section 2 (b) section 5

Fig. 18. Lateral variation of $(UV)_d$ and k for 16/01/2008.

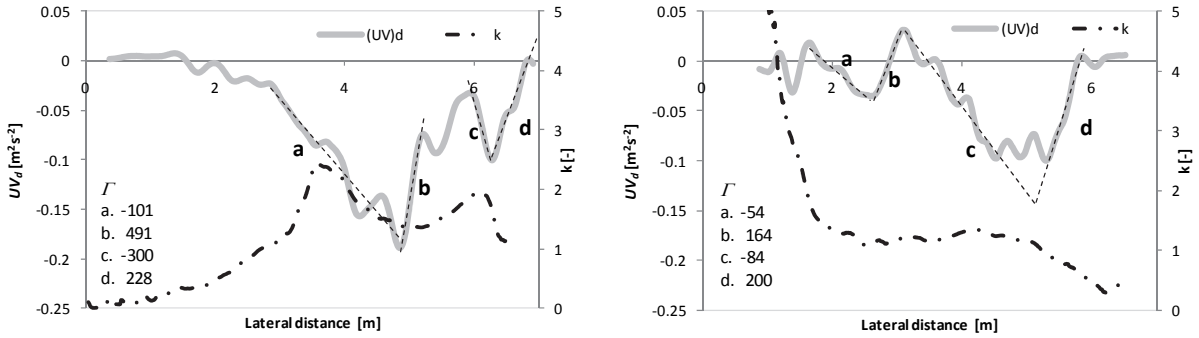

(a) section 2 (b) section 5

Fig. 19. Lateral variation of $(UV)_d$ and k for 10/02/2009.

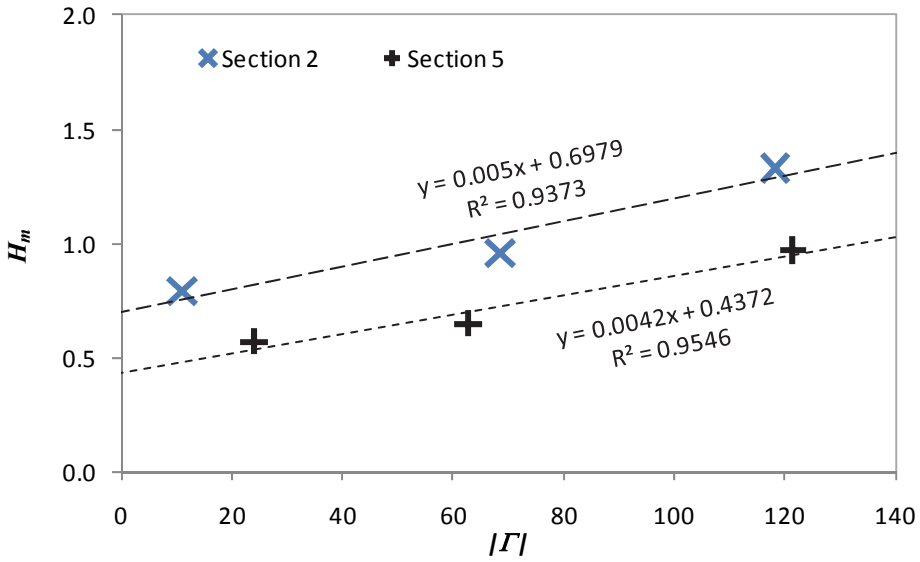

Fig. 20. Relationship between $\overline{|\Gamma|}$ and H_m.

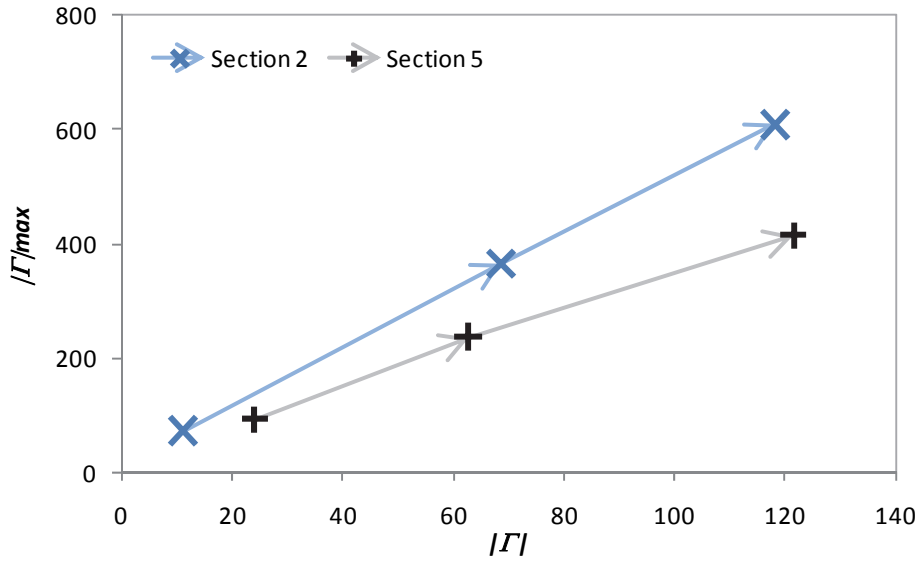

Fig. 21. Relationship between $\overline{|\Gamma|}$ and $|\Gamma|_{\max}$.

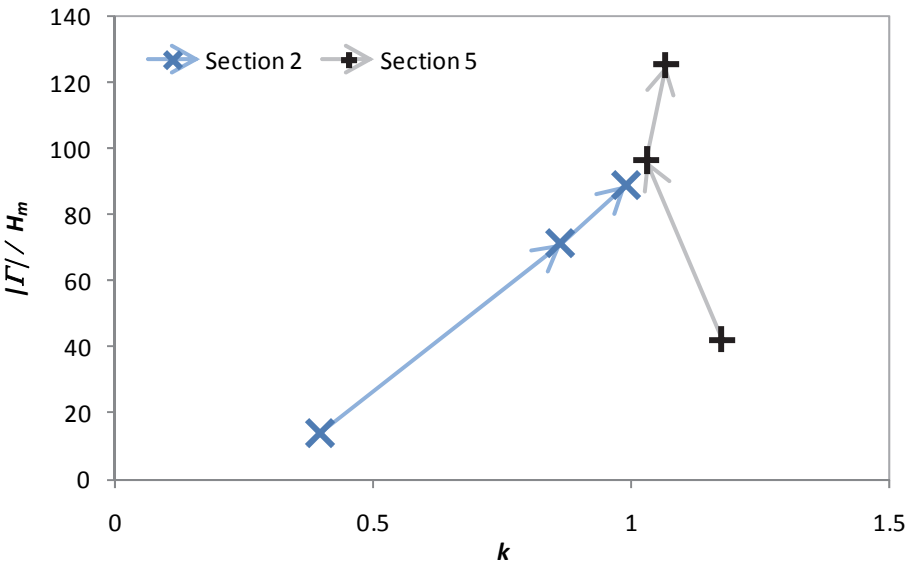

Fig. 22. Normalised secondary flow term versus the velocity index.

Figure Captions

Fig. 1. A schematic illustrating the possible relationship between the depth averaged and surface streamwise velocities.

Fig. 2 Cross section and staff gauge locations.

Fig. 3 Cross sectional profiles: (a) cross section 2; (b) cross section 5

Fig. 4 Water level elevations relating to the three fieldwork campaigns: (a) 16/01/2008 inbank data; (b) 18/08/2008 bankful data; (c) 10/02/2009 overbank data.

Fig. 5 Water level elevations at six measurement stations during five fieldwork campaigns

Fig. 6. Photographs illustrating changes in vegetation with respect to time (flow event).

Fig. 7. Contours of the streamwise velocity component (*U)* for the three dates of concern – cross section 2. (y is the lateral distance from the left hand bank looking downstream).

Fig. 8. Contours of the streamwise velocity component (*U)* for the three dates of concern – cross section 5. (y is the lateral distance from the left hand bank looking downstream).

Fig. 9. Velocity vectors at cross section 5 for 10/02/09 flood event.

Fig. 10. Secondary flow circulations for the three flow events – cross section 2.

Fig. 11. Secondary flow circulations for the three flow events – cross section 5.

Fig. 12 Comparison of ADCP streamwise velocity and PIV surface velocity for 16/01/2008 inbank flow case (U_d (ADCP) – solid line, U_s (PIV) dashed grey line, U_d/U_s –doubled dashed grey line).(a) section 2; (b) section 5.

Fig. 13 Comparison of ADCP streamwise velocity and PIV surface velocity for 18/08/2008 bankful flow case.(a) section 2; (b) section 5.

Fig. 14 Comparison of ADCP streamwise velocity and PIV surface velocity for 10/02/2009 overbank flow case. (a) section 2; (b) section 5.

Fig. 15. Depth-averaged secondary flow [22].

Fig. 16. Depth-averaged secondary flow parameter [22].

Fig. 17. Lateral variation of Γ and k for 18/08/2008.

Fig. 18. Lateral variation of Γ and k for 16/01/2008.

Fig. 19. Lateral variation of Γ and k for 10/02/2009.

Fig. 20. Relationship between $\overline{|\Gamma|}$ and H_m.

Fig. 21. Relationship between $\overline{|\Gamma|}$ and $|\Gamma|_{\max}$.

Fig. 22. Normalised secondary flow term versus the velocity index.